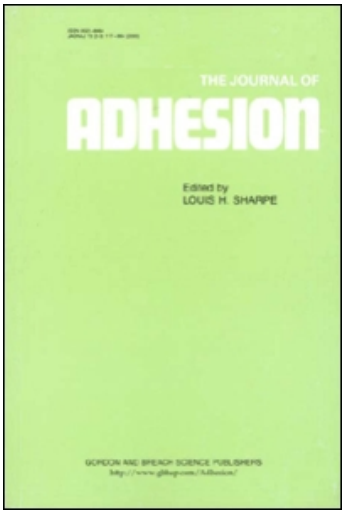

The Journal of Adhesion

Publication details, including instructions for authors and subscription information:
http://www.informaworld.com/smpp/title~content=t713453635

Effect of Bondline Thickness on Mixed-Mode Debonding of Adhesive Joints to Electroprimed Steel Surfaces

D. W. Schmueser[a]; N. L. Johnson[a]
[a] Engineering Mechanics Department, RMB-256, General Motors Research Laboratories, Warren, MI, U.S.A.

To cite this Article Schmueser, D. W. and Johnson, N. L.(1990) 'Effect of Bondline Thickness on Mixed-Mode Debonding of Adhesive Joints to Electroprimed Steel Surfaces', The Journal of Adhesion, 32: 2, 171 — 191
To link to this Article: DOI: 10.1080/00218469008030189
URL: http://dx.doi.org/10.1080/00218469008030189

J. Adhesion, 1990, Vol. 32, pp. 171–191
Reprints available directly from the publisher
Photocopying permitted by license only

Printed in the United Kingdom

Effect of Bondline Thickness on Mixed-Mode Debonding of Adhesive Joints to Electroprimed Steel Surfaces†

D. W. SCHMUESER and N. L. JOHNSON

Engineering Mechanics Department, RMB-256, General Motors Research Laboratories, Warren, MI 48090-9055, U.S.A.

(Received February 9, 1989; in final form April 30, 1990)

Structural applications of adhesive bonding have been increasing in recent years due to improvements in the types of adhesives available and in improved knowledge of bonding procedures. Consequently, there exists a demand for techniques to assess adhesive joint strength, particularly along bondline interfaces where compliant adhesives contact more rigid metallic surfaces. The present study investigates the mixed-mode response of cracked-lap-shear (CLS) joints bonded with unprimed and electroprimed steel adherend surfaces. Three bondline thicknesses, representative of structural automotive joints, were evaluated for unprimed and primed bondlines. Experimental results for static load *versus* debond extension were input to finite element analyses for computing debond parameters (strain energy release rates). The debonds always initiated at a through-the-thickness location that had the greatest peel component of strain energy release rate. The total strain energy release rate values correlated well with trends in joint strength as a function of bondline thickness.

KEY WORDS Cracked-lap-shear joint; finite element analysis; electropriming; strain energy release rate; bondline interface.

INTRODUCTION

Recent studies[1,2] conducted at General Motors Research Laboratories have shown that bonding to electroprimed steel surfaces has enhanced strength characteristics compared with conventional bonds to unprimed steel surfaces. The priming process consists of depositing a thin layer of zinc phosphate crystals onto a steel ferric oxide surface. A layer of organic primer is then deposited onto the zinc phosphate. A primed surface formed in this manner can be referred to as an "ELPO" surface, the term "ELPO" referring to the electrodeposition of organic primer. By using a properly formulated adhesive, strengths for single-lap-shear (SLS) joints showed increases of up to 30 percent on ELPO-primed steel compared with strengths for unprimed steel bondlines. Subsequent computational

† Presented at the Twelfth Annual Meeting of The Adhesion Society, Inc., Hilton Head Island, South Carolina, February 20–22, 1989.

studies based on finite element analyses of varied SLS joint moduli and thicknesses have provided an explanation for the enhanced strength characteristics of ELPO-primed joints. The presence of the primer reduced peak peel and shear stresses and allowed for a more uniform stress distribution throughout the joint.

While the SLS joint geometry is useful for qualification testing and for comparing static strengths for different adhesive formulations and surface treatments, its usefulness for developing failure criteria for bonded joints is limited by highly nonlinear stress behavior[3] and the inability to represent different ratios of peel-to-shear response. Such control of mixed-mode behavior is needed to develop accurate failure criteria for bonded joints subjected to static and cyclic loads.

Unlike the SLS specimen, the cracked-lap-shear (CLS) specimen, illustrated in Figure 1, is capable of representing mixed-mode joint behavior for large area bonds that are typical of many structural applications. Both peel and shear stresses are present in the bondline of this joint. The magnitude of each component of this mixed-mode joint behavior can be modified by changing the relative thicknesses of the lap and strap adherends. Previous studies have applied the CLS joint geometry to investigate the static[4] and cyclic[5–7] debond behavior of

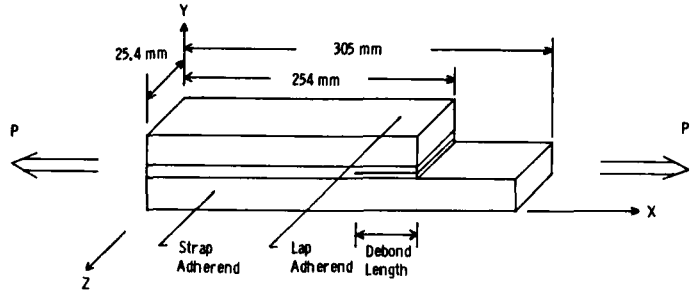

a) Load Configuration

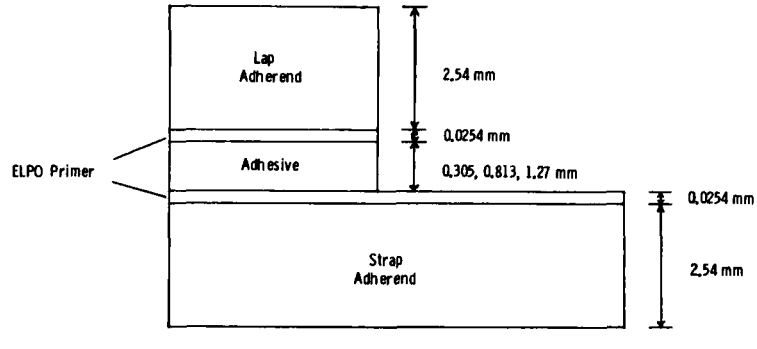

b) Bondline Thickness

FIGURE 1 CLS joint geometry.

composite-to-metal and composite-to-composite joints. All of these studies were directed at joints having bondline thickness values typical of aerospace structures (0.076–0.203 mm). However, adhesive bondlines for automotive structural applications typically range from 0.254 mm to 1.27 mm. Thus, the purpose of the present study was to examine the effects of bondline thickness on the mixed-mode response of unprimed and primed mild steel CLS joints. Three bondline thicknesses were evaluated: 0.305, 0.813, and 1.27 mm. Static loads were considered for this initial phase of the study. Subsequent work will be directed toward debonding of cyclically-loaded CLS joints.

The following sections describe the experimental and computational procedures that were applied to determine the mixed-mode response of the unprimed and primed joints.

EXPERIMENTAL CHARACTERIZATION OF BONDLINE MATERIALS AND CLS JOINT STRENGTH

The adhesive used for this study was Ciba-Geigy's Araldite XB 3131, a one-part epoxy adhesive. The ELPO-primer was PPG Industry's Uniprime 3150A, a proprietary formulation used in GM manufacturing facilities. Tensile properties of the primer material were obtained by testing coupon samples of the thin material removed from a primed surface with a sharp blade. The $102 \times 13 \times 0.2$ mm specimens were tested at room temperature in accordance with ASTM D882, using an Instron Model 1125 machine at a crosshead speed of 3 mm/min. Serrated grips were used in conjunction with pressure-sensitive tape tabs to secure the specimens. Specimen extension was measured by grip separation. Tensile adhesive specimens were cut from cast sheets of XB 3131 adhesive. The $254 \times 25 \times 3$ mm specimens were tested at room temperature in accordance with ASTM D638, using an MTS Model 810 machine at a crosshead speed of 3 mm/min. Rigid end labs were employed to reinforce the ends of the mechanically-gripped coupons. Moduli for the primer and adhesive materials, calculated from the initial slope of the stress-strain curves, are listed in Table I.

Equal thickness (2.54 mm), mild 1010 steel adherends were used for the CLS joints. The lengths of the strap and lap adherends were 305 and 254 mm, respectively (Fig. 1a). The relative thicknesses of the adhesive and primer layers in the bonded specimens are illustrated in Fig. 1b. Unprimed CLS specimens

TABLE I
Adhesive and ELPO-primer elastic moduli

Material	Modulus (GPa)	Adhesive/ELPO modulus ratio
One-part epoxy (XB-3131)	2.83	2.18
ELPO primer	1.3	—

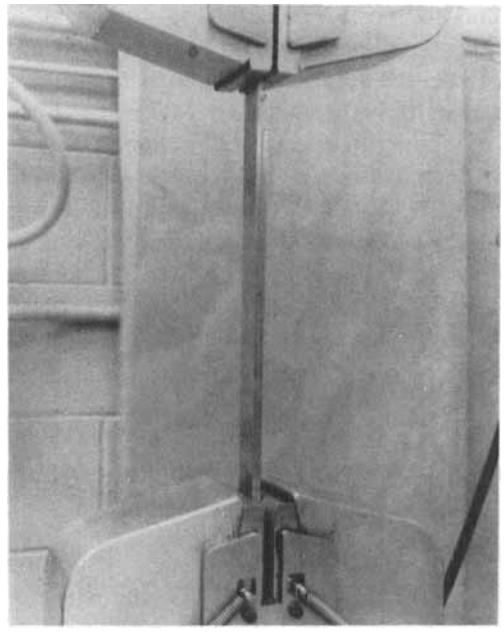

FIGURE 2 CLS test configuration.

were cut from steel panels that had been degreased with trichloroethane. For the primed specimens, the steel panels were zinc-phosphated before the ELPO-priming process was completed. Steel wires with diameters equal to 0.254 mm, 0.762 mm, and 1.27 mm were used as spacers to maintain uniform bondline thickness for the cured panels. The specimens were tested on an MTS Model 810 machine at a crosshead speed of 1.0 mm/min under load control conditions, as illustrated in Figure 2. The extent of the joint debond zone was determined

TABLE II
CLS test results for 0.305 mm bondline thickness

Unprimed specimens					
Test No. 1		Test No. 2		Test No. 3	
a (mm)	P (kN)	a (mm)	P (kN)	a (mm)	P (kN)
3.175	9.786	3.175	12.454	3.175	13.344
4.763	12.899	6.35	15.123	4.763	14.678
9.525	14.234	9.525	15.568	6.35	15.123
15.875	18.236	15.875	18.236	12.7	17.347
ELPO-Primed specimens					
Test No. 1		Test No. 2		Test No. 3	
a (mm)	P (kN)	a (mm)	P (kN)	a (mm)	P (kN)
3.175	13.344	3.175	13.344	3.175	12.010
4.763	13.789	6.35	13.789	4.763	13.789
9.525	17.792	9.525	16.013	6.35	15.123
19.05	19.126	15.875	18.682	12.7	17.347

TABLE III
CLS Test Results for 0.813 mm Bondline Thickness

Unprimed Specimens					
Test No. 1		Test No. 2		Test No. 3	
a(mm)	P(kN)	a(mm)	P(kN)	a(mm)	P(kN)
3.175	13.344	4.763	12.454	3.175	14.678
6.35	14.234	6.35	13.789	6.35	16.012
9.525	15.123	12.7	14.678	7.938	16.902
12.7	16.458	15.875	15.568	9.525	18.237
ELPO-Primed Specimens					
Test No. 1		Test No. 2		Test No. 3	
a(mm)	P(kN)	a(mm)	P(kN)	a(mm)	P(kN)
4.763	16.013	3.175	15.568	4.763	15.123
6.35	16.458	7.938	16.902	7.938	16.458
7.94	17.792	15.875	17.347	9.525	17.792
12.7	18.237	19.05	18.237	12.7	18.682

optically (visually) with a 20X microscope and graduated scale. Tests for each bondline thickness for the primed and unprimed joints were repeated three times. Tables II–IV summarize the loads and debond growth results.

The possible failure modes in a statically-loaded steel joint are adherend failure (metal yield), cohesive failure within the adhesive, or adhesive failure at a bond interface. All specimens in the present study failed adhesively. The unprimed joints failed at the adhesive/steel interface (Figure 3a) while the ELPO-primed joints failed at the ELPO/steel interface (Fig. 3b). A possible qualitative explanation for this debond behavior can be determined by computing strain energy release rate components G_i and G_{ii} at selected locations through the

TABLE IV
CLS test results for 1.27 mm bondline thickness

Unprimed specimens					
Test No. 1		Test No. 2		Test No. 3	
a (mm)	P (kN)	a (mm)	P (kN)	a (mm)	P (kN)
3.175	13.344	3.175	12.9	3.175	12.454
6.35	14.234	6.35	14.234	9.525	15.568
12.7	15.123	7.938	14.678	15.875	16.012
19.05	16.012	9.525	15.123	—	—
ELPO-primed specimens					
Test No. 1		Test No. 2		Test No. 3	
a (mm)	P (kN)	a (mm)	P (kN)	a (mm)	P (kN)
3.175	16.012	3.175	16.012	4.763	16.012
6.35	16.458	12.7	16.458	7.938	16.458
12.7	16.902	15.875	18.237	12.7	16.902
19.05	19.126	19.05	18.682	15.875	18.682

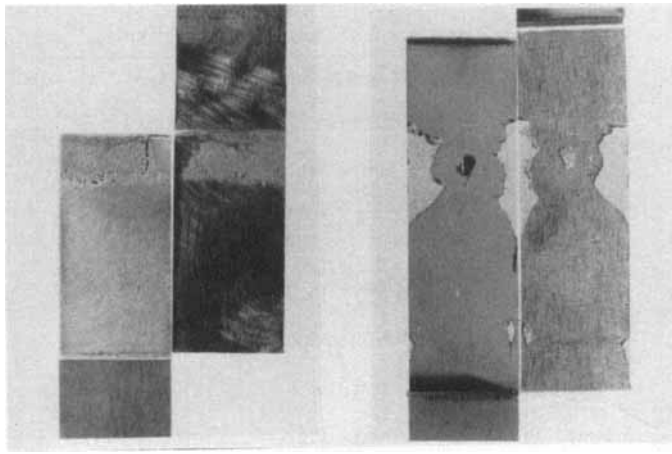

FIGURE 3 Failure characteristics for unprimed and ELPO-primed specimens.

adhesive thickness and at the bondline material interfaces. A previous analysis[1] of the SLS joint showed that debond location could be qualitatively correlated with trends in the through-the-thickness values of the component strain energy release rates. This same approach will be applied in the following sections to the CLS joint.

COMPUTATIONAL ANALYSIS

The CLS joint geometries were analyzed with finite element techniques for given bondline thickness, debond length, and applied load. Plane strain, two-dimensional analyses were completed. The analyses accounted for geometric nonlinearities that are associated with large rotations that occur in the strap/lap debond area. Two numerical techniques—one based on a singular finite element (SFE) method[8] for modeling the crack tip region, and another based on a virtual crack extension (VCE) method[9]—were used to compute strain energy release rates. The following presents a brief description of the finite element modeling procedures and the two techniques for computing strain energy release rates.

Finite element modeling procedures

Previous parametric studies[10] have shown that the selection of boundary conditions can have a significant effect on the computation of stress distributions and strain energy release rates in an adhesively bonded joint. The boundary conditions employed for the CLS finite element analyses are illustrated in Figure 4. Constraints are placed at the fixed and loaded ends of the joint to simulate the grip conditions used in the experiments.

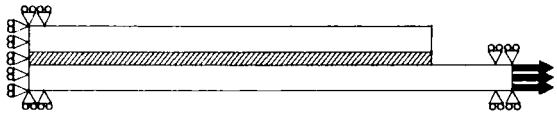

FIGURE 4 Boundary conditions and load application for finite element analyses.

The singular finite element (SFE) method uses eight-node isoparametric elements in regions remote from the debond front and eight, six-node triangular elements of the variable singularity type[8] at the debond front. The singular element is conformable with adjacent eight-node isoparametric elements. A typical finite element model for the CLS specimen using the SFE technique consisted of 1212 isoparametric elements. Five elements with a nonuniform through-the-thickness distribution were used to model the adherend thickness. Four elements were used to model the ELPO layer. The number of elements employed to model the adhesive bondline thickness was seventeen, determined from the mesh sensitivity study described in the next section.

The VCE technique[9] relies on a fine density of four-node isoparametric elements to compute component strain energy release rates. The finite element meshes used for this study consisted of approximately 3400 elements. Nonuniform meshes consisting of ten elements were used to model the adherend thickness, while three elements were used to model the ELPO-layer thickness. Nonuniform meshes consisting of 5, 12, and 24 elements were applied to model adhesive bondline thicknesses equal to 0.254, 0.803, and 1.27 mm, respectively.

Formulations for mixed-mode debond parameters

Debond parameters that describe mixed-mode behavior of the CLS joint are the total strain energy release rate, G_t, and its components, G_i and G_{ii}, the opening and shear mode release rates, respectively. The SFE and VCE methods employ different formulations to determine the mixed-mode parameters. However, both formulations make use of displacement fields near the debond tip. The SFE method is based on a formulation originally derived by Smelser.[11] Crack flank displacements along the upper and lower debond faces are needed to apply this method. Displacements near the debond front are represented in a six-node singular finite element as

$$u = C_u r^{1/2}, \qquad v = C_v r^{1/2} \tag{1}$$

where the coefficients C_u and C_v are determined directly from the finite element solution along rays which correspond to the sides of the singular elements surrounding the crack tip (Figure 5). The u and v displacements in Eq. (1) correspond to sliding and opening crack flank displacements for the cartesian coordinate shown in Figure 5. The crack opening displacements can then be calculated as

$$\Delta u = (C_u^+ - C_u^-)r^{1/2}, \qquad \Delta v = (C_v^+ - C_v^-)r^{1/2} \tag{2}$$

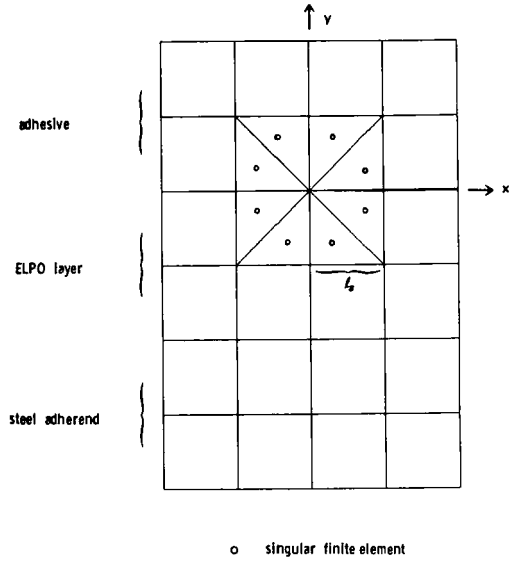

FIGURE 5 Computational model for singular finite element (SFE) method.

where the plus and minus superscripts signify the upper and lower debond face, respectively.

The total strain energy release rate as a function of component stress intensity factors, K_i and K_{ii}, was determined by Smelser to be of the form

$$G_t = \tfrac{1}{16}(\Lambda_1 + \Lambda_2)(K_i^2 + K_{ii}^2) \tag{3}$$

where Λ_1 and Λ_2 are defined in the Appendix.

The component values of G_t, G_i, and G_{ii}, can be computed as functions of the C_u and C_v coefficients. Previous work directed at applying Smelser's formulation to the SLS joint[1] derived expressions for G_t, G_i, and G_{ii} which are functions of ΔC_u and ΔC_v defined in Eq. (2), and K_i and K_{ii}. These expressions, summarized below, are used for computing parameters for the CLS joints.

$$G_t = \frac{2\lambda_0^2}{(\Lambda_1 + \Lambda_2)}\{\Delta C_u^2 + \Delta C_v^2\} \tag{4}$$

$$G_i = \tfrac{1}{16}[\Lambda_1 + \Lambda_2]K_i^2 \tag{5}$$

$$G_{ii} = \tfrac{1}{16}[\Lambda_1 + \Lambda_2]K_{ii}^2 \tag{6}$$

The parameters λ_0, K_i, and K_{ii} in Eqs. (4)–(6) are defined in the Appendix. Concepts for using these parameters in elastic analysis of interface cracks have been summarized in a study by Rice.[12] The above formulation for the SFE method has been incorporated into the finite element code VISTA.[13] The VISTA program was used in this study to apply the SFE method to analyze the CLS specimens.

The VCE method is based on a formulation originally derived by Rybicki and Kanninen.[9] The technique is based on the total strain energy release rate given by

the following expression in polar coordinates.

$$G_t = \lim_{\Delta a \to 0} \frac{1}{2\Delta a} \int_0^{\Delta a} [\sigma_y(\Delta a - r, 0)\, \Delta v(r, \pi) + \tau_{xy}(\Delta a - r, 0)\, \Delta u(r, \pi)]\, dr \quad (7)$$

where σ_y and τ_{xy} are stresses ahead of the debond tip (located at $r = 0$), Δu and Δv are the relative sliding and opening displacements between points on the debond faces, and Δa is the crack extension at the debond tip.

The first and second integrals in Eq. (7) are the Mode I and Mode II components, respectively. Thus, for a virtual crack extension we have

$$G_i = \lim_{\Delta a \to 0} \frac{1}{2\Delta a} \int_0^{\Delta a} \sigma_y(\Delta a - r, 0)\, \Delta v(r, \pi)\, dr \quad (8)$$

$$G_{ii} = \lim_{\Delta a \to 0} \frac{1}{2\Delta a} \int_0^{\Delta a} \tau_{xy}(\Delta a - r, 0)\, \Delta u(r, \pi)\, dr. \quad (9)$$

The integration of Eqs. (8) and (9) can be performed numerically or analytically using forces and displacements at the element nodes. The GAMNAS[14] computer program, used in this study to apply the VCE method to the CLS joints, uses the latter approach based on forces transmitted across the crack tip and relative opening and sliding displacements ahead of the debond tip. Based on the transformed coordinates illustrated in Figure 6, the equations used in GAMNAS to compute G_i and G_{ii} are

$$G_i = \frac{1}{2} P_{\bar{y}} \cdot \frac{[\bar{v}_2 - \bar{v}_3]}{\Delta a} \quad (10)$$

$$G_{ii} = \frac{1}{2} P_{\bar{x}} \cdot \frac{[\bar{u}_2 - \bar{u}_3]}{\Delta a} \quad (11)$$

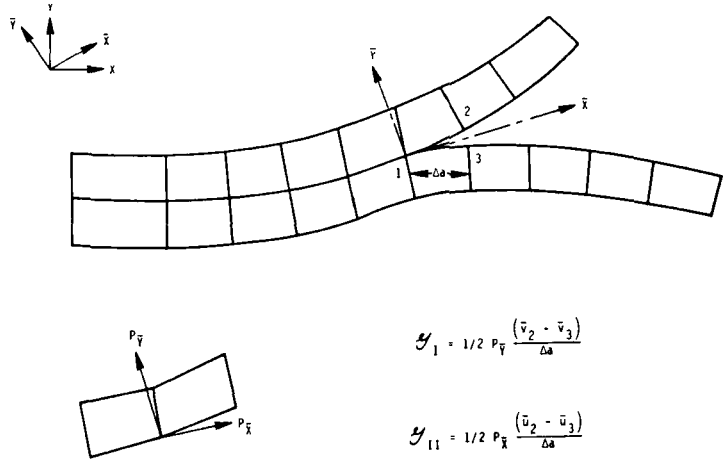

FIGURE 6 Element formulation for the virtual crack extension (VCE) technique.

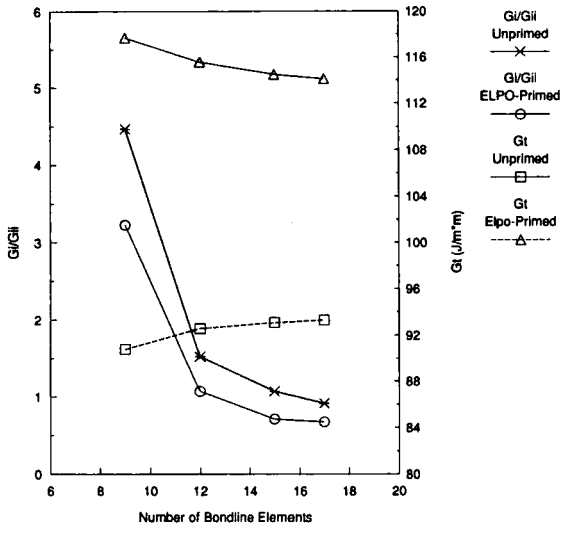

FIGURE 7 Through-the-thickness mesh size dependence of G_t and G_i/G_{ii} (bondline thickness = 0.305 mm, a = 3.175 mm).

These expressions are derived from estimations[9] of nodal forces and are valid only for linear and geometrically nonlinear analyses.

Previous studies[1,15] have shown computations for G_i and G_{ii} to be more sensitive to mesh size at the debond tip than are computations for G_t. Therefore, a mesh size sensitivity study was conducted for the CLS geometries to determine the influence of the number of through-the-thickness elements on G_{ii} and mode mix (G_i/G_{ii}). The results of the study for the SFE formulation are illustrated in Figure 7. While results for G_t are relatively insensitive to mesh size, the G_i/G_{ii} ratio is strongly dependent on mesh size. As a result of this study, 17 elements were used to model the bondline thickness for the SFE method. This corresponds to an l_s value of 0.00635 mm for the side of the singular element shown in Figure 5. A similar sensitivity study for the VCE technique gave a Δa (Figure 6) value equal to 0.0076 mm for computing the strain energy release rates with the GAMNAS code.

COMPUTATIONAL RESULTS FOR STRAIN ENERGY RELEASE RATES

Computational studies were completed to determine the effect of the ELPO priming on the magnitudes of the total strain energy release rate and on the relative magnitude of opening mode to shearing mode. Load *versus* debond length data were input into the VISTA and GAMNAS codes to compute strain energy release rate values. Although, as previously discussed, these programs employ different formulations to compute G_i and G_{ii}, the values for G_t determined from these programs should be equal. The results plotted in Figure 8

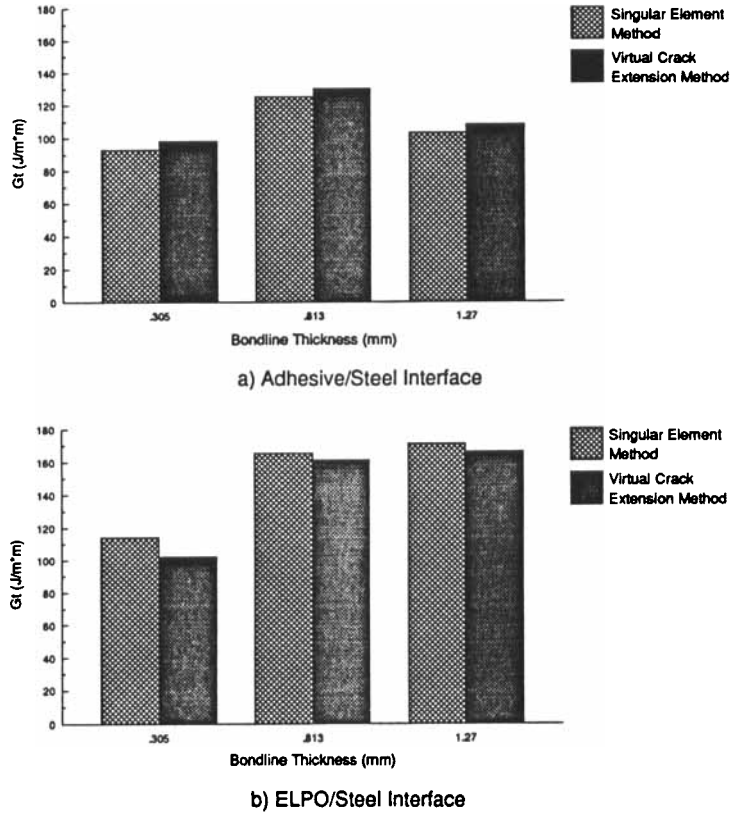

FIGURE 8 Variation of G_t with bondline thickness for singular finite element and virtual crack extension methods.

show that this is indeed the case for the three bondline thicknesses considered for this study. The maximum difference between the computational results for a debond length of 3.175 mm was for the thin bondline case for the unprimed joint. For this case the VCE technique was 12 percent lower than the SFE method.

All of the specimens for this study failed either at the adhesive/steel interface (unprimed joints) or at the ELPO/steel interface (primed joints). Although a quantitative determination of the actual debond path for the multi-material interface bondline cannot be made from strain energy release rate analyses, a relative comparison of trends in G_t and G_i at selected bondline interfaces can qualitatively reveal the influence of peel behavior on the debond location. Using the finite element techniques previously described, strain energy release rates G_t and G_i were calculated at the adhesive/ELPO and ELPO/steel interfaces. Analysis results are presented in Figure 9 for these interfaces. Since the SFE and VCE techniques were shown previously to give similar results for G_t, only results corresponding to the SFE method are illustrated in Figure 9. The averaged ratio of G_t at the ELPO/steel interface to that at the adhesive/steel interface was 1.18

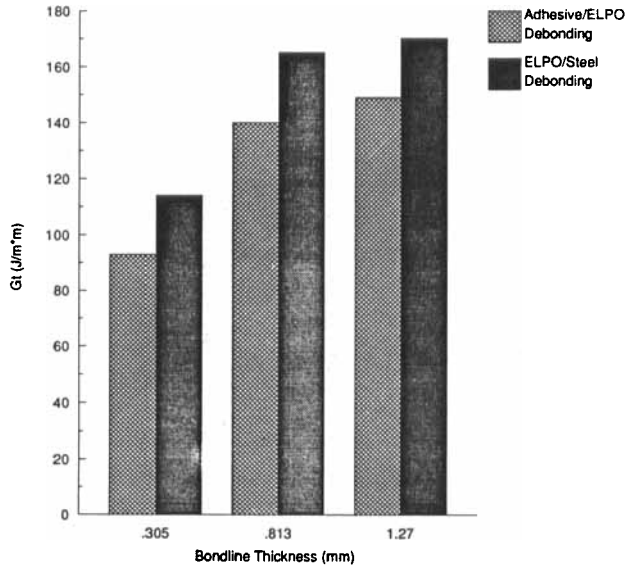

FIGURE 9 Effect of debond location on G_t values for the singular finite element formulation.

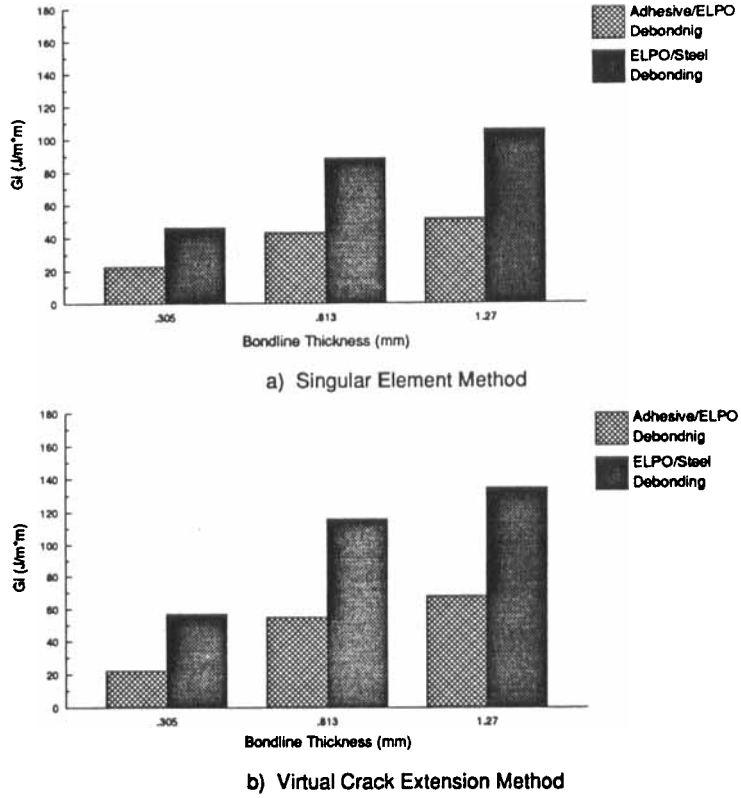

FIGURE 10 Effect of debond location on peel behavior of primed joints.

for the three bondline thicknesses. Since adhesives are usually weaker under peel loading than under shear loading, G_i values at the interfaces were also computed. Figure 10 shows the results of these G_i computations for the two computational methods considered in this study. The averaged ratios for G_i at the ELPO/steel interface to values at the adhesive/ELPO interface were 2.05 and 2.23 for the SFE and VCE methods, respectively. These results indicate that G_i has a greater influence on debond location than does G_t. This result is consistent with the observation of other researchers.[7]

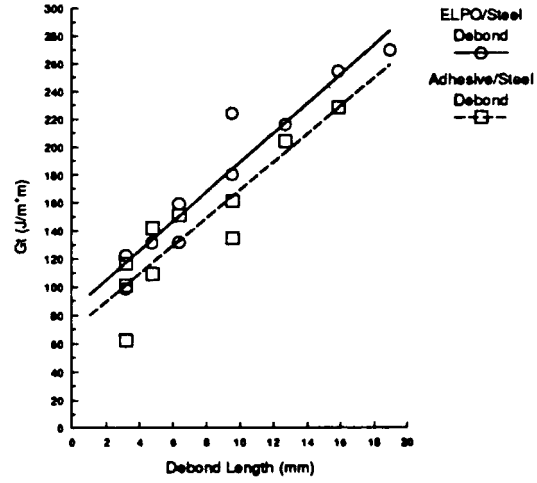

a) Bondline Thickness = 0.305 mm

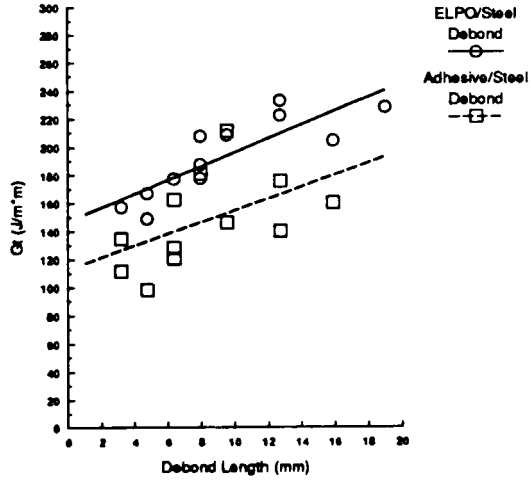

b) Bondline Thickness = 0.813 mm

FIGURE 11 Variation of G_t with debond length for three bondline thicknesses based on the singular finite element formulation.

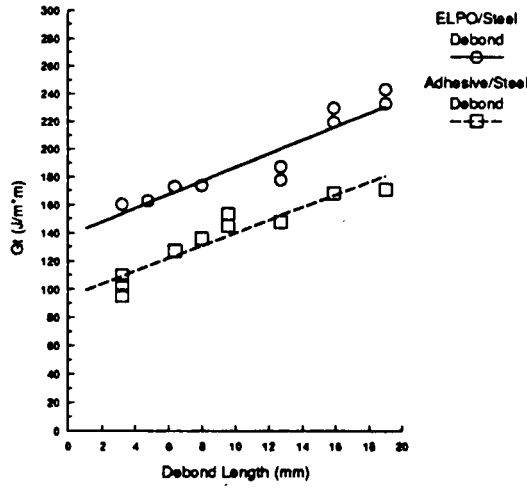

c) Bondline Thickness = 1.27 mm

FIGURE 11 (*continued*)

Computational results for G_t versus debond length are illustrated in Figure 11 for the three bondline thicknesses considered for this study. The G_t values correlated well with trends in joint strength as a function of bondline thickness. As illustrated in Figure 11, the ELPO-primed CLS joints showed significant increases in total release rate values as the bondline thickness was increased. Specifically, averaged G_t values corresponding to a debond length of 3.175 mm were increased by 32, 51, and 64 percent for bondline thicknesses equal to 0.305, 0.813, and 1.27 mm, respectively. The largest values for G_t occurred for the 0.813 mm bondline thickness.

Nondimensionalized G_i values are illustrated in Figure 12 for unprimed and primed joints for a debond length equal to 3.175 mm. The nondimensionalized values were computed using the equation

$$\bar{G}_i = G_i \left\{ \frac{2E_1E_2}{[E_1(1-\nu_2^2) + E_2(1-\nu_1^2)]\sigma_i^2 \pi a} \right\} \tag{12}$$

where E_α and ν_α are Young's modulus and Poisson's ratio, respectively, for the upper ($\alpha = 1$) and lower ($\alpha = 2$) material at the debond interface. The stress applied to the CLS joint is represented by σ_i, while the debond length is given by a. These results show a significant reduction in non-dimensionalized Mode I for the primed joints compared with the unprimed joints. G_i decreased by an average of 54 percent for the SFE results. These reductions in peel response, which account for different joint debond loads, are directly related to the enhanced strengths of the CLS joints.

While results for G_t compare favorably between the SFE and VCE methods, significant differences exist for the G_i and G_{ii} strain energy release rates. The through-the-thickness variance of G_i/G_{ii} is illustrated in Figure 13 for a CLS joint

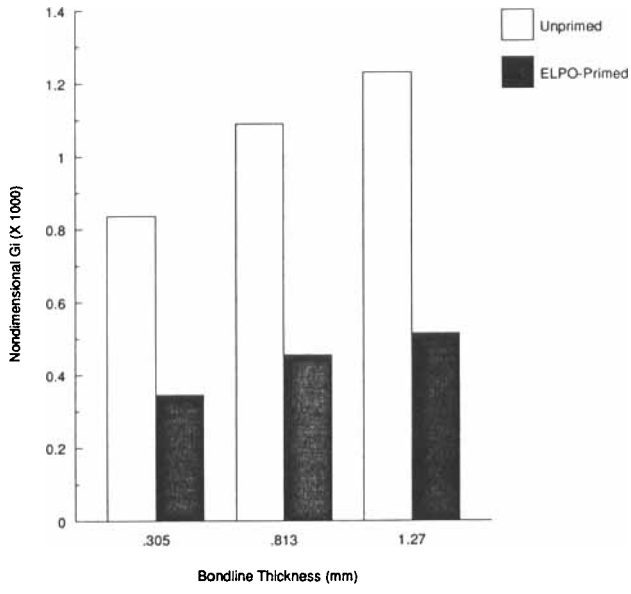

FIGURE 12 Nondimensionalized G_i values for unprimed and primed joints based on the singular finite element formulation ($a = 3.175$ mm).

with a bondline thickness equal to 0.305 mm and a crack length of 3.175 mm. The mode mix ratio was computed as selected distances from the adherend/primer or adherend/adhesive interface. If H_c/H denotes the ratio of this distance (H_c) to the bondline thickness (H), then release rates for ratios equal to 0.5, 0.2, 0.1, 0.05, and 0.0 (adhesive debonding) were determined. As shown in Fig. 13, the SFE and VCE methods give comparable results when the bondline is located at the middle of the adhesive layer ($H_c/H = 0.5$). These H_c/H values compare favorably with values reported by Johnson[16] for an ASTM round robin analysis of the CLS specimen. However, as the through-the-thickness debond location is brought closer to the adherend/adhesive interface, differences in the component release rate values are evident. The SFE method gives greater G_i/G_{ii} values for the unprimed joints compared with the primed joints. The VCE method, on the other hand, predicts significantly greater G_i/G_{ii} values for the primed joints compared to the unprimed joints. Differences between the two methods are greatest at $H_c/H = 0.0$, as summarized in Table V. G_i values computed by applying the VCE method were a factor of 1.5 less than G_i values computed from the SFE formulation for unprimed CLS joints. The corresponding factor for peel behavior of the primed joints was 0.8. The trends were reversed for the shear release rate components. Similar results were reported by Ginsburg[15] when applying the two methods to a point-loaded blister specimen. Since the shear modulus of the ELPO is approximately one-half the adhesive shear modulus, one would expect more shear deformation and greater G_{ii} values for the primed joints. Dattaguru *et al.*[17] showed that this is indeed the case when examining

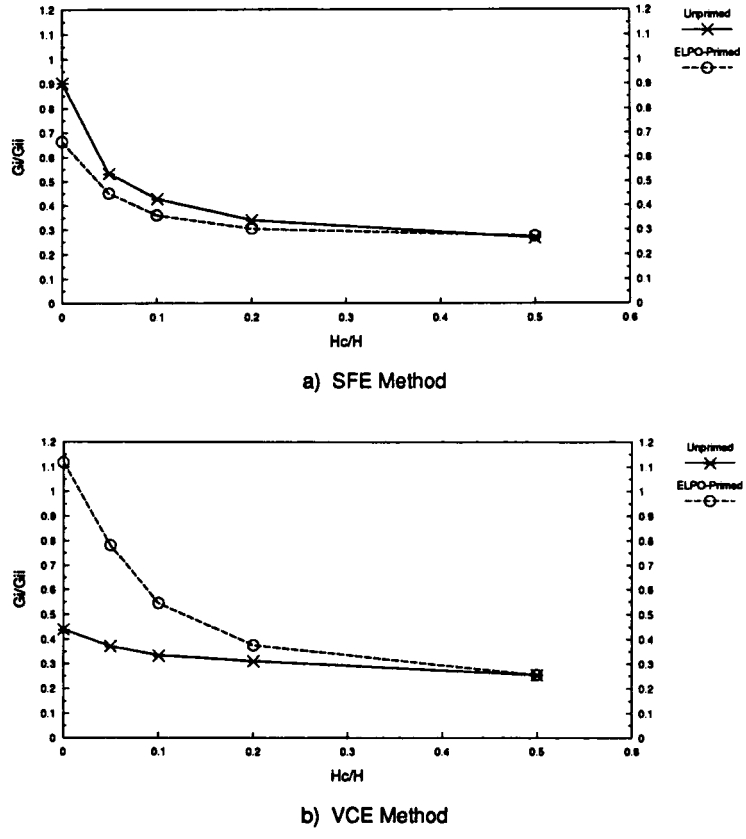

FIGURE 13 Variation of G_i/G_{ii} through the bondline thickness (bondline thickness = 0.305 mm, a = 3.175 mm).

the effects of adhesive modulus on strain energy release rates for a composite/aluminum CLS joint.

The reason for the significant differences in G_i/G_{ii} predictions between the SFE and VCE methods is a matter of definition. In the SFE formulation (Eqs. (5–6)), G_i and G_{ii} are associated with K_i^2 and K_{ii}^2, respectively. However, for the VCE method (Eqs. (8–9)), the crack front stresses and displacements both are functions of K_i and K_{ii}, as discussed by Rice.[12] Therefore, G_i values based on Δv and the product $\sigma_y \Delta w$ will contain K_i^2, K_{ii}^2, and $K_i K_{ii}$ terms. A similar analysis can be applied to G_{ii} defined in Eq. (9). Thus, in view of the computational results and the definitions for G_i and G_{ii}, the component strain energy release rate values computed using the SFE method represent changes in debond deformation characteristics between primed and unprimed CLS joints more realistically at a debond interface than those computed using the VCE method. The SFE and VCE methods give comparable mode-mix results at the middle of the adhesive bondline.

TABLE V
Comparison of component strain energy release rate results for SFE and VCE methods
(Bondline Thickness = 0.305 mm, a = 3.175 mm)

SFE method

Unprimed specimens					ELPO-primed specimens				
Test No.	G_i (J/m^2)	G_{ii} (J/m^2)	G_t (J/m^2)	G_i/G_{ii}	Test No.	G_i (J/m^2)	G_{ii} (J/m^2)	G_t (J/m^2)	G_i/G_{il}
1	29.7	32.1	61.8	0.92	1	49.2	73.3	122.5	0.67
2	48.2	52.8	101.0	0.91	2	49.2	73.3	122.5	0.67
3	55.4	61.0	116.4	0.91	3	40.0	58.7	98.7	0.68
Avg.	44.4	48.6	93.1	0.91	Avg.	46.1	68.4	114.6	0.67

VCE method

Unprimed specimens					ELPO-primed specimens				
Test No.	G_i (J/m^2)	G_{ii} (J/m^2)	G_t (J/m^2)	G_i/G_{ii}	Test No.	G_i (J/m^2)	G_{ii} (J/m^2)	G_t (J/m^2)	G_i/G_i
1	18.0	40.9	58.9	0.44	1	59.7	50.2	109.9	1.19
2	30.3	66.8	97.1	0.45	2	59.7	50.2	109.9	1.19
3	41.5	95.9	137.4	0.43	3	47.7	40.8	88.5	1.17
Avg.	29.9	67.9	97.8	0.44	Avg.	55.7	47.1	102.8	1.18

CONCLUSIONS

The CLS specimen represents a simple structural joint that exhibits both peel and shear response when subjected to in-plane loads. The present study has investigated the mixed-mode response of CLS joints bonded with unprimed and ELPO-primed adherend surfaces. Three different bondline thicknesses (0.305, 0.813, and 1.27 mm) were evaluated for the unprimed and primed joints. Debond parameters (strain energy release rates) were computed based on the SFE and VCE methods. Experimental results for load and debond extension were input to finite element analyses for computing the debond parameters. The CLS specimens failed in an adhesive mode either at the adhesive/steel interface (unprimed joints) or at the ELPO/steel interface (primed joints). The failure location was independent of bondline thickness. However, the debond always grew at a through-the-thickness location that had the greatest peel (G_i) component of strain energy release rate. Thus, qualitatively, the peel response of the joint had a stronger influence on the debond location than did the total strain energy release rate, G_t.

The G_t values correlated well, however, with the trends in joint strength as a function of bondline thickness. Unprimed CLS joints showed initial increases in strength when bondline thickness was increased from 0.305 to 0.813 mm. The strengths decreased significantly when the thickness was further increased to 1.27 mm. In contrast, the primed joints had increases in bond strength for each increase in thickness. However, ELPO-priming was most effective at enhancing the strength of the thickest CLS joints. Experimental bondline strengths increased by 8.7, 11.1, and 24.1 percent for bondline thicknesses equal to 0.305, 0.813, and 1.27 mm, respectively.

In general, adhesive joints are inherently weaker when placed under peel loads than when placed under shear loads. Results obtained for nondimensionalized G_i values corresponding to unprimed and primed joints are consistent with this general trend. Significant reduction in peel response (54 percent) of the ELPO-primed joint is directly related to the enhanced strengths of the primed joints.

Finally, while computational results for G_t compare favorably between the SFE and VCE techniques, results for component release rates G_i and G_{ii} do not compare well. The VCE method did not predict anticipated increases in shear response (Mode II) of the joints when a softer ELPO-primer layer was placed in the bondline. The SFE formulation, on the other hand, predicted increasing Mode II response for the ELPO-primed joints. These trends are consistent with results cited from the literature and with the definitions of the two computational methods.

Acknowledgments

The authors would like to thank Jack Melichar of General Motors Research Labs for designing the specimen grips and Carol Megal of Ciba-Geigy for providing the one-part epoxy adhesive.

References

1. D. W. Schmueser, "Strain Energy Release Rate Characterization of Structural Adhesive Bonds to Primer Electrodeposited on Steel," in *Advances in Adhesively Bonded Joints, ASME MD-Vol. 6,* S. Mall, K. M. Liechti, and J. R. Vinson, Eds. (American Society of Mechanical Engineers, New York, 1988), p. 101.
2. D. W. Schmueser, N. L. Johnson, and R. T. Foister, *J. Adhesion* **24,** 47 (1987).
3. J. A. Harris and R. D. Adams, *Int. J. Adhesion and Adhesives* **4,** 65 (1984).
4. T. R. Brussat, S. T. Chiu, and S. Mostovy, "Fracture Mechanics for Structural Adhesive Bonds," AFML-TR-163 (1977).
5. S. Mall, M. Rezaizadeh, and R. Gurumurthy, *J. Eng. Mat. and Tech.* **109,** 17 (1987).
6. W. S. Johnson and S. Mall, "A Fracture Mechanics Approach for Designing Adhesively Bonded Joints," in *Delamination and Debonding of Materials, ASTM STP 876,* W. S. Johnson, Ed. (American Society for Testing and Materials, Philadelphia, 1985), p. 189.
7. S. Mall, W. S. Johnson, and R. A. Everett, Jr., "Cyclic Debonding of Adhesively Bonded Composites," in *Adhesive Joints,* K. L. Mittal, Ed. (Plenum Publishing Co., New York, 1984), p. 639.
8. M. Stern, *J. Numer. Meth. in Engg.* **14,** 409 (1979).
9. E. F. Rybicki and M. F. Kanninen, *Engg. Fract. Mechs.* **9,** 931 (1977).
10. J. N. Reddy and S. Roy, "Finite Element Analysis of Adhesively Bonded Joints," Virginia Tech VPI-E-85.18, (August 1988).
11. R. L. Smelser, *Int. J. Fracture* **15,** 135 (1979).
12. J. R. Rice, *J. Applied Mechanics* **55,** 98 (1988).
13. E. B. Becker, R. S. Chambers, L. R. Collins, W. G. Knauss, K. M. Liechti, and J. Romanko, "Viscoelastic Analysis of Adhesively Bonded Joints Including Moisture Diffusion," AFWAL-TR-84-4057, (1984).
14. J. D. Whitcomb and B. Dattaguru, "User's Manual for Gamnas—Geometric and Material Nonlinear Analysis of Structures," NASA TM 85734, (January 1984).
15. D. Ginsburg, "Calculations of Fracture Parameters for Interface Cracks with Application to Mixed Mode Crack Initiation," University of Texas EMRL-87/2, (1987).
16. W. S. Johnson, *J. of Testing and Evaluation* **15,** 303 (1987).
17. B. Dattaguru, R. A. Everett, Jr., J. D. Whitcomb, and W. S. Johnson, *J. Engg. Matls And Tech.* **104,** 59 (1984).

Appendix

A debond extending along the interface between two elastic, isotropic materials can be idealized as an interface crack consisting of an upper debond face ($\alpha = 1$) and a lower debond face ($\alpha = 2$). As shown by Smelser[11] a complex stress intensity factor, K, for characterizing the stress field near the debond tip is given by

$$K = K_0 e^{i\beta} = K_i + iK_{ii} \tag{13}$$

where K_i and K_{ii} are stress intensity components corresponding to opening and shearing modes, respectively.

These components can be decomposed into

$$\begin{aligned} K_i &= K_0 \cos\beta \\ K_{ii} &= K_0 \sin\beta \end{aligned} \tag{14}$$

where

$$K_0 = [K_i^2 + K_{ii}^2]^{1/2} = \frac{4\sqrt{2}\,\lambda_0}{(\Lambda_1 + \Lambda_2)} \left[\frac{\Delta^2 v + \Delta^2 u}{r}\right]^{1/2} \tag{15}$$

$$\beta = \varepsilon \ln r_0 - \delta - \pi/2 - \Phi\,|_{r_0} \tag{16}$$

$$\tan\Phi = \Delta v/\Delta u \tag{17}$$

and r_0 is an arbitrary location at which the components of crack opening displacement, Δv and Δu, are determined.

The constant λ_0 is expressed as

$$\lambda_0 = \tfrac{1}{2}(1 + 4\varepsilon^2)^{1/2} \tag{18}$$

where ε is the bi-material elastic constant defined by

$$\varepsilon = \frac{1}{2\pi} \ln\left[\frac{\mu_1 + \mu_2 K_1}{\mu_2 + \mu_1 K_2}\right] \tag{19}$$

and

$$K_\alpha = \begin{Bmatrix} 3 - 4\nu_\alpha & \text{Plane Strain} \\ (3 - \nu_\alpha)/(1 + \nu_\alpha) & \text{Plane Stress} \end{Bmatrix}, \qquad \alpha = 1, 2 \tag{20}$$

In Eqs. (19)–(20), μ_α and ν_α are the shear modulus and Poisson's ratio of material α, respectively.

Furthermore, the material constants Λ_α in Eq. (15) are defined as

$$\Lambda_\alpha = \begin{Bmatrix} 4(1 - \nu_\alpha)/\mu_\alpha & \text{Plane Strain} \\ 4/\mu_\alpha(1 + \nu_\alpha) & \text{Plane Stress} \end{Bmatrix}, \qquad \alpha = 1, 2 \tag{21}$$

while the δ constant in Eq. (16) is defined as

$$\delta = \tan^{-1}(2\varepsilon) \tag{22}$$

Thus, the individual stress intensity components can be computed using Eqs. (14)–(22) once Δu and Δv have been determined from the displacement field at a distance r_0 from the debond tip.

Very close to the crack tip the displacements along the upper and lower debond surfaces have the form

$$u = C_u r^{1/2}, \qquad v = C_v r^{1/2} \tag{23}$$

The coefficients C_u and C_v are determined directly from singular crack tip elements.[8] The crack opening displacements can then be calculated as

$$\Delta v = (C_v^+ - C_v^-) r^{1/2}, \qquad \Delta u = (C_u^+ - C_u^-) r^{1/2} \tag{24}$$

where the plus and minus superscripts denote the upper and lower debond surfaces, respectively.

Using Eqs. (14)–(15) and Eq. (24), the component stress intensity factors can be expressed as

$$K_i = \frac{4\sqrt{2}\,\lambda_0}{\Lambda_1 + \Lambda_2} (\Delta C_u^2 + \Delta C_v^2)^{1/2} \cos\beta \tag{25}$$

$$K_{ii} = \frac{4\sqrt{2}\,\lambda_0}{\Lambda_1 + \Lambda_2} (\Delta C_u^2 + \Delta C_v^2)^{1/2} \sin\beta \tag{26}$$

Using these expressions for K_i and K_{ii}, the total energy release rate can be expressed as

$$G_t = \tfrac{1}{16} (\Lambda_1 + \Lambda_2)(K_i^2 + K_{ii}^2) \tag{27}$$

Substituting Eqs. (25)–(26) into Eq. (27) gives G_t in terms of the crack flank displacement coefficients

$$G_t = \frac{2\lambda_0^2}{\Lambda_1 + \Lambda_2} (\Delta C_u^2 + \Delta C_v^2). \tag{28}$$

The determination of K_i and K_{ii} involves an arbitrary length parameter, r_0, which appears in the definitin of β (Eq. 16). Even though r_0 and ε in Eq. (20) are very small in magnitude, the $\varepsilon \ln r_0$ term is of the same order as $\pi/2$ and Φ.

Thus, K_i and K_{ii} can vary over selected regions for computing the stress intensity factors. However, the total strain energy release rate is independent of r_0. For the CLS joints considered in this study, a sensitivity study showed that an r_0 value equal to 0.025 μm was appropriate for computing the debond parameters using Eqs. (25)–(27).

For the case of cohesive debonding (crack front between similar materials), it can be shown that component values given by Eqs. (25)–(26) are independent of r_0. The material constants for cohesive debonding reduce to

$$\varepsilon = \delta = 0, \qquad \lambda_0 = 1/2 \tag{29}$$

Thus,

$$\beta = \left[\frac{\pi}{2} + \tan^{-1}(\Delta C_v/\Delta C_u)\right] \tag{30}$$

$$\cos\beta = \cos[\tan^{-1}(\Delta C_v/\Delta C_u)]$$

$$= \frac{\Delta C_v}{(\Delta C_v^2 + \Delta C_u^2)^{1/2}} \tag{31}$$

Similarly,

$$\sin\beta = \frac{\Delta C_u}{(\Delta C_v^2 + \Delta C_u^2)^{1/2}} \tag{32}$$

Thus, substituting Eqs. (29)–(32) into Eqs. (25)–(26) gives the following strain energy release rate components for a cohesive bond.

$$G_i = \frac{1}{\Lambda}(\Delta C_v^2) \tag{33}$$

$$G_{ii} = \frac{1}{\Lambda}(\Delta C_u^2) \tag{34}$$

Using Eq. (21) for plane strain and the following relationship between shear modulus and Young's modulus

$$\mu = \frac{E}{2(1+\nu)}, \tag{35}$$

Equations (33) and (34) reduce to

$$G_i = \frac{E\,\Delta C_v^2}{32(1-\nu^2)} \tag{36}$$

$$G_{ii} = \frac{E\,\Delta C_u^2}{32(1-\nu^2)} \tag{37}$$